Low-Dimensional Materials
https://www.sciltp.com/journals/ldm

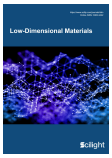

Article

Flexible Nanofiber Moisture-Enabled Electric Generator Based on Horizontal Asymmetric Structure

Maoshuang Ran [1], Chunqiao Fu [1], Xulei Lu [1,*] and Tingting Yang [1,2]

[1] Tribology Research Institute, School of Mechanical Engineering, Southwest Jiaotong University, Chengdu 610031, China
[2] Institute of Smart City and Intelligent Transportation, Southwest Jiaotong University, Chengdu 611756, China
* Correspondence: lu_xulei@my.swjtu.edu.cn

How To Cite: Ran, M.; Fu, C.; Lu, X.; et al. Flexible Nanofiber Moisture-Enabled Electric Generator Based on Horizontal Asymmetric Structure. *Low-Dimensional Materials* **2026**, *2*(1), 1. https://doi.org/10.53941/ldm.2026.100001

Received: 29 October 2025
Revised: 4 January 2026
Accepted: 5 January 2026
Published: 12 January 2026

Abstract: Harvesting electricity from atmospheric humidity represents a highly promising pathway for clean energy conversion. However, conventional nanofiber-based moisture-enabled electric generators mostly rely on vertical humidity gradients to generate power, leaving horizontally structured moisture-enabled electric generators relatively unexplored. Herein, we report a flexible moisture-induced electricity generator based on an electrospun polyacrylonitrile (PAN) nanofiber membrane, which achieves self-driven potential output through horizontally asymmetric distribution of sodium dodecyl benzene sulfonate (SDBS). Specifically, the nanofiber membrane was dip-coated with carbon nanotubes (CNT/PAN), not only introducing multi-level porous nanochannels but also endowing it with sensitive perception of ion migration. Subsequently, one half of the CNT/PAN was immersed in an SDBS solution to construct an asymmetric moisture-capturing structure, enabling the device to induce an ion concentration gradient upon humidity exposure. The gradient drives ion migration, thereby generating an ionic current. Under 93% relative humidity (RH), the device achieves an open-circuit voltage of 60 mV and a short-circuit current of 3 μA. The designed device can not only generate electricity but also function as a self-powered humidity sensor for applications such as touch sensing. It delivers stable direct-current output from ambient humidity without any external energy input, exhibiting good moisture response and promising wearability. These findings may provide new insights into the design and application of horizontally structured nanofiber-based moisture-enable electric generators.

Keywords: electrospinning; moisture electricity; horizontal asymmetric structure

1. Introduction

With the escalating global energy crisis and environmental pollution, the development of renewable and clean energy conversion and harvesting technologies has become a central focus in energy science research. Compared to traditional green energy sources—such as wind, solar, and thermal power [1–3], which are often constrained by geographical and environmental limitations, moisture-enabled electric generators (MEGs) have gained significant attention in recent years. In particular, MEGs stand out due to the ubiquitous nature of atmospheric humidity. To date, extensive research and optimization have been conducted on various materials for this purpose, including carbon-based materials [4–8], metal oxides [9,10], biomass [11–16], and polymers [17–20]. Among these, flexible porous polymer membranes have become a research focus in moisture energy conversion, owing to their excellent processability, tunable porosity, and designable interfacial properties, which enable precise regulation of ion transport pathways [21–24]. Electrospinning, a widely used technique for producing nanofibers from polymer

solutions, has been frequently employed to fabricate MEGs, as the resulting nanofibers possess abundant surface functional groups and a high specific surface area [25–27].

Currently, most electrospun MEGs adopt a sandwich-like vertical configuration—typically comprising a top electrode, a moisture-sensitive membrane, and a bottom electrode—where electricity is generated via ion transport across the thickness direction. This vertical design often maximizes contact area and separation efficiency, thereby delivering relatively high power output. For instance, Sun et al. developed a sandwich-structured MEG using a pair of oppositely charged electrodes and an electrolyte-loaded electrospun nanofiber membrane [28]. The device generates electrical signals through the differential attraction of cations and anions by the charged electrodes, a mechanism attributed to capacitive effects. In another study, Wang et al. constructed a MEG based on an electrospun membrane incorporating oxidized silk fibroin and silver nanoparticles (AgNPs) [21], also following a sandwich architecture. Their device leverages the inherent humidity gradient between a porous top electrode and a solid bottom electrode, combined with the negatively charged fiber backbone, to induce selective ion migration and cation–anion separation, thereby producing electricity. In contrast, horizontally structured MEGs integrate all functional components on the same plane or substrate. This monolithic design offers greater structural integrity, mechanical stability, and enhanced resistance to bending, stretching, and impact, potentially leading to longer device lifetimes. A comparison of the advantages and disadvantages between horizontal and vertical structures is summarized in Table S1 (see Supplementary Materials). It can be concluded that horizontal MEGs offer distinct advantages in terms of mechanical robustness, packaging reliability, and integration potential, as well as adaptability to emerging energy harvesting modes such as droplet-based energy conversion. Nevertheless, research on horizontally structured MEGs remains relatively limited [29].

In this study, we fabricate a horizontal asymmetric moisture-enabled electric generator (HAMEG) based on a PAN electrospun nanofiber membrane modified with carbon nanotubes (CNT) and featuring a horizontally asymmetric SDBS distribution. First, the PAN membrane was repeatedly immersed in a CNT ethanol dispersion and dried, forming a conductive network on the fiber surfaces that significantly enhances the membrane's responsiveness to ion migration signals. Subsequently, half of the membrane was selectively immersed in an SDBS aqueous solution, creating a spatial asymmetry in the hygroscopic SDBS distribution. This structure establishes a macroscopic ion gradient between the two lateral ends and, at the microscopic level, a stable ionic potential difference within the fibrous channels. Upon exposure to humidity, the SDBS-rich side absorbs moisture and dissociates, releasing Na^+ ions. Concurrently, the hydrolysis of the nitrile groups on the PAN fibers renders the membrane surface negatively charged. As a result, cations migrate from the high-concentration side to the low-concentration side under the combined influence of the concentration gradient and the electric double layer, leading to spatial separation of cations and anions and the generation of an electrical potential. These mechanisms have been verified through scanning electron microscopy (SEM), energy-dispersive X-ray spectroscopy (EDS), and systematic electrical measurements.

Compared to conventional electrospun moisture-electric devices, the HAMEG exhibits the following distinctive features: (1) The incorporation of CNTs yields a micro–nano hierarchical porous structure within the nanofiber network, providing abundant ion transport channels and facilitating efficient ion conduction; (2) The conductive pathways formed by CNT modification ensure stable signal transmission, which is essential for electricity generation. Meanwhile, the asymmetric distribution of hygroscopic SDBS guarantees a humidity gradient across the device and contributes to the formation of an ion concentration gradient, forming the fundamental basis for moisture-enabled power generation. The device ultimately achieves an output of 60 mV and 3 μA. Moreover, this horizontally asymmetric generator highlights the critical role of conductive material coating in such planar configurations and elucidates the energy conversion mechanism based on the synergy between ion migration and the microstructure. The fabrication process is straightforward, requiring neither complex electrode patterning nor high-temperature treatment, and the device exhibits excellent flexibility and scalability. Compared with advanced patterning techniques such as 3D printing and inkjet printing, the electrospinning–impregnation strategy offers higher material compatibility, intrinsic multiscale porosity, and facile scalability, making it particularly suitable for flexible moisture-enabled energy harvesting devices [30–33]. This strategy offers a new perspective for developing flexible moisture energy harvesters with controllable structures and high stability.

2. Method

2.1. The Manufacturing Process of Electrospun Films

A 10 wt% spinning solution was prepared by dissolving polyacrylonitrile (PAN, Mw = 45,000) in N, N-dimethylformamide (DMF, 99%). The resulting PAN solution was loaded into a 30 mL syringe. Electrospinning was carried out under the following conditions: an applied voltage of 17 kV, a collection distance of 15 cm, and a

solution feed rate of 1 mL/h. The process was conducted at a temperature of 25 ± 3 °C and a relative humidity of 30 ± 5% RH. The as-prepared PAN nanofiber membrane was subsequently dried at 60 °C for 6 h to remove any residual solvent. The detailed experimental procedure is schematically illustrated in Figure 1.

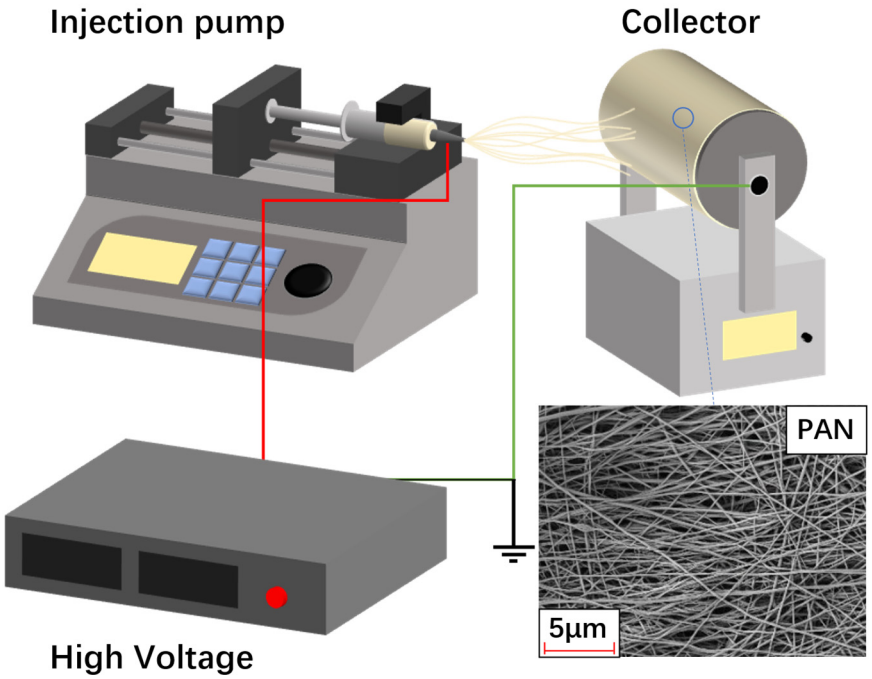

Figure 1. Flowchart and scan electron microscope diagram of preparing nanofiber films by electrospinning.

2.2. The Manufacturing Process of Flexible Moisture-Based Generators

First, 100 mg of carbon nanotubes (CNTs) were dispersed in 300 mL of anhydrous ethanol and treated using an ultrasonic cell crusher (Yilong 92-II, Shanghai Yilong Co., Ltd., Shanghai, China) for 0.5 h to form a uniformly dispersed suspension for subsequent use. Subsequently, 1 g of sodium dodecyl benzene sulfonate (SDBS, Mw~348.48) was dissolved in 30 mL of deionized water to form a clear solution.

The as-prepared CNT suspension was then applied to the PAN electrospun membrane via dip-coating, with the number of dipping cycles used to control the loading amount. After each dip-coating step, the membrane was dried in an oven at 80 °C for approximately 5 min. The same dip-coating and drying procedure was subsequently performed using the SDBS solution on the resulting PAN/CNT membrane. The detailed fabrication process is schematically illustrated in Figure 2.

Finally, carbon wires attached with conductive carbon tape were connected to both ends of the membrane to serve as electrodes. The side of the membrane not treated with SDBS was sealed with adhesive tape.

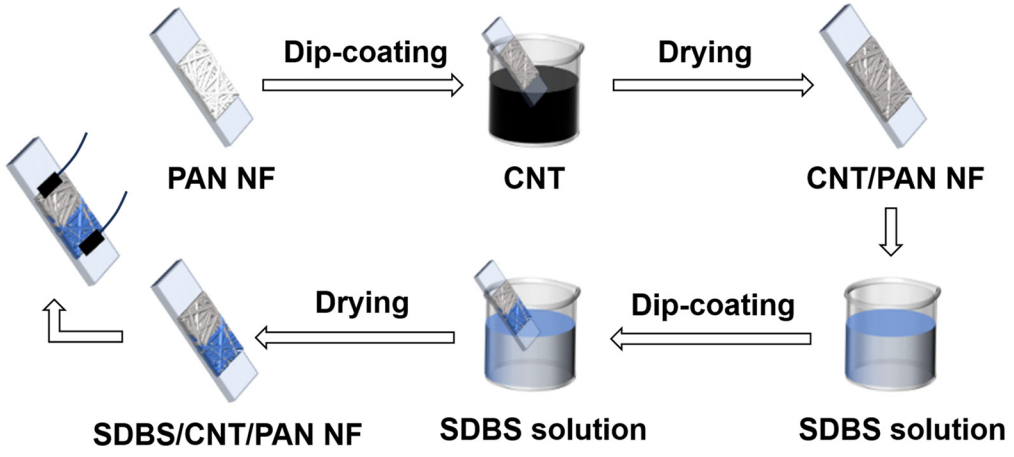

Figure 2. Flowchart for the production of HAMEG.

2.3. Performance Measurement and Characterization

The electrical output performance, including open-circuit voltage (V_{OC}) and short-circuit current (I_{SC}), was recorded in real-time using a digital source meter (Keithley 2450, Keithley Instruments, Solon, OH, USA). The surface morphology and elemental distribution of the SDBS/CNT/PAN composite membrane were characterized by scanning electron microscopy (SEM) (ZEISS Sigma 360, Carl Zeiss AG, Germany). Furthermore, the zeta potentials of the SDBS solution and CNT suspension were measured with a high-sensitivity zeta potential and particle size analyzer (Nano ZS, Malvern Instruments, Malvern, UK), while the surface zeta potential of the pristine PAN nanofiber membrane was determined using a solid surface zeta potential analyzer (SurPASS 3, Anton Paar, Graz, Austria). X-ray photoelectron spectroscopy (XPS) (ESCALAB QXi, Thermo Fisher Scientific, Brno, Czech Republic) was employed to investigate the chemical structure of PAN nanofiber membranes after CNT impregnation, while Fourier transform infrared spectroscopy (FT-IR) (Nicolet iS50, Thermo Fisher Scientific, Waltham, MA, USA) was used to analyze and compare the chemical structures of pristine PAN membranes and SDBS-impregnated PAN membranes.

3. Result

To construct a flexible substrate and establish initial ion transport channels, a PAN nanofiber membrane was first prepared via electrospinning (details are provided in Figure S1). As shown in Figure 3a, the pristine PAN nanofiber membrane exhibits a porous structure with large inter-fiber spaces. After three cycles of dip-coating in a CNT ethanol dispersion followed by thorough drying, the CNTs uniformly filled the interstitial spaces between the PAN fibers (see Figures S2 and S3), introducing nanoscale pores within the nanofiber membrane [34]. This resulted in a hierarchical pore architecture that facilitates the rapid transport of water molecules and ions (Figure 3b). Subsequently, through three cycles of local impregnation and drying on one side of the membrane using an SDBS aqueous solution, SDBS was successfully incorporated into the nanofibers (see Figure S4) and an asymmetric moisture-absorbing structure was constructed (Figure 3c). As the PAN molecular chains contain –C≡N groups, which hydrolyze to release protons and leave a negatively charged backbone [35], and considering the inherent electronegativity of CNTs, the overall membrane channels possess a negative surface charge. This characteristic is essential for the selective migration of cations (Figure 3d). The overall schematic of the device is shown in Figure 3e, with the membrane size being 2×4 cm^2 in the study. The resulting membrane possesses multi-scale channels spanning micro- and nano-dimensions, which not only provide hierarchical pathways for moisture and ion transport but also promote ion migration rates [36]. Furthermore, the negative surface charge of the membrane grants it cation selectivity, establishing a prerequisite for the directional transport of cations. When combined with aluminum electrodes, the device generated a current output of 3 μA under a humid environment (93% RH), as shown in Figure 3e. Under optimized conditions, a power density of 43.3 nW/cm^2 was obtained at a load resistance of 10 kΩ (see Figure S5). To evaluate the performance level of our device, we have summarized the performance of recently reported MEGs in Table S2. As shown, while the output of the proposed HAMEG is lower than that of some recent state-of-the-art MEGs, its performance nonetheless remains within the top tier among electrospinning-based devices. While aluminum electrodes yield a higher apparent output, carbon electrodes were utilized for quantitative characterization to suppress parasitic redox contributions from the electrodes. This approach ensures a more accurate assessment of the intrinsic moisture-induced ion transport mechanism. Saturated salt solutions were used throughout the experiments to maintain a stable humidity level. The testing environment and the corresponding relative humidity levels achieved by different salt solutions are provided in Figures S6 and S7.

Subsequent tests were conducted using carbon electrodes to better investigate the operational mechanisms and influencing factors of the electricity generation. First, the influence of nanofiber membrane thickness on the output performance was examined. The electrospinning duration determines the membrane thickness, which increases with increasing spinning time. Figure 4a shows the short-circuit current characteristics of devices fabricated with different electrospinning times (with both CNT and SDBS dip-coating repeated three times). The performance initially increased and then decreased with increasing thickness, reaching an optimum at a spinning time of 6 h. Excessively short spinning times (e.g., 2 h) resulted in poor film formation, making it difficult to support the attachment of CNT and SDBS; therefore, such samples were excluded from further testing. Overly long spinning times (e.g., 8 h) led to excessive membrane thickness, hindering the transport of ions and water molecules and consequently reducing the output signal, indicating that overly thick nanofiber membranes are unfavorable for ion and water migration. Therefore, nanofiber membranes spun for 6 h were selected for subsequent experiments. In addition, the influence of the film length and width on the device performance was

also discussed (see Figures S8 and S9). For the subsequent experiments, a film length of 4 cm and width of 2 cm were selected.

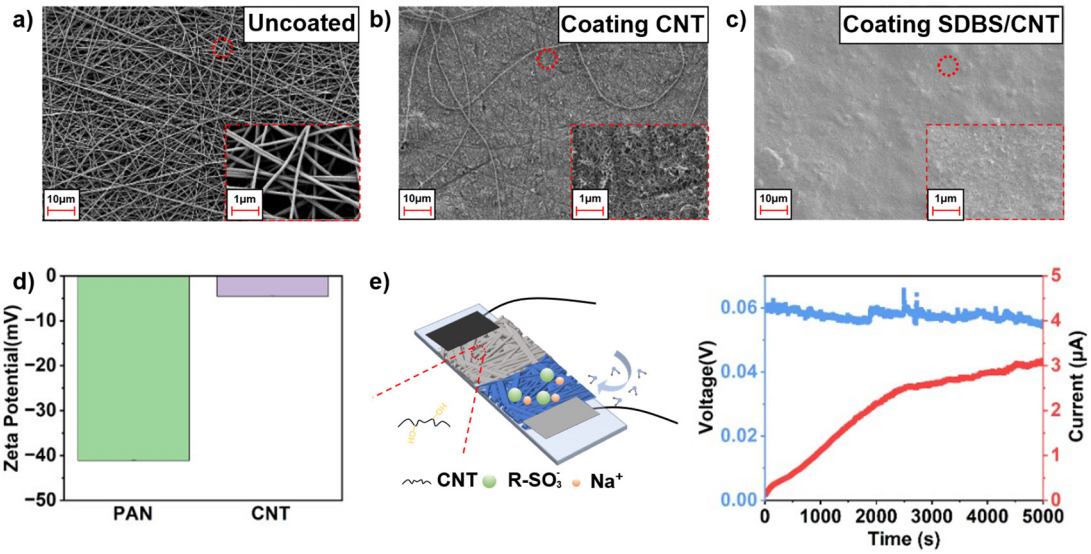

Figure 3. Relevant characterization and schematic diagram of flexible HAMEG. (**a**) The SEM image of the initial PAN nanofiber film. (**b**) SEM image of CNT/ PAN nanofiber film. (**c**) SEM images of SDBS/CNT/PAN nanofiber films. (**d**) Zeta potential of PAN nanofiber films and CNT suspensions. (**e**) Schematic diagram of flexible moisture-based generator and related performance of using aluminum electrodes.

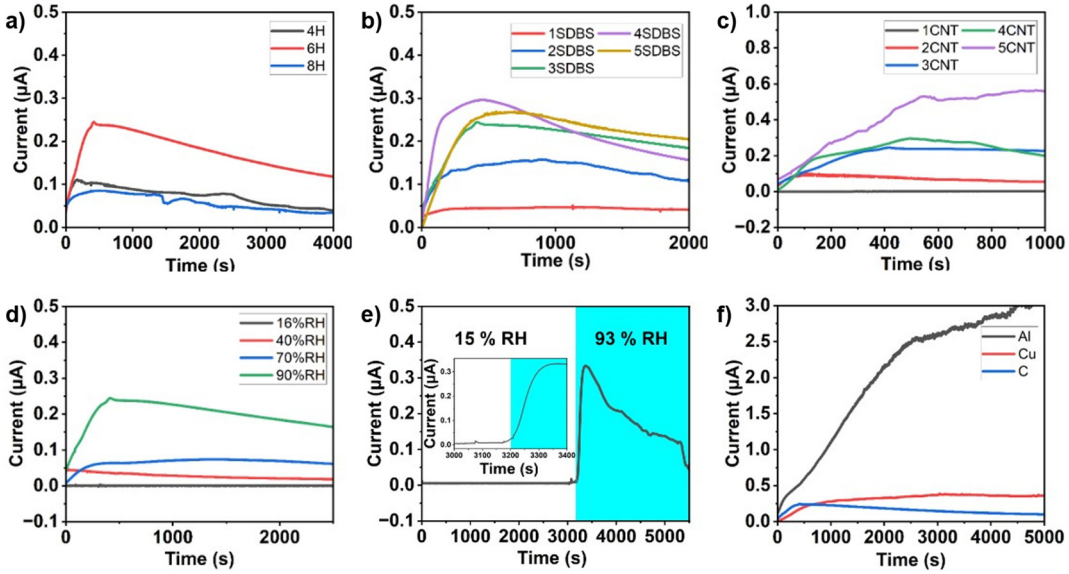

Figure 4. Parameters affecting the performance of flexible HAMEG. (**a**). Short-circuit current output of devices with different film thicknesses. (**b**) Short-circuit current output under different SDBS dip-coating times. (**c**) Short-circuit current output under different CNT dip-coating times. (**d**) Short-circuit current output under different humidity conditions. (**e**) Short-circuit current output under sudden changes in humidity from 15% to 93%. The illustration is a partial enlargement of Figure 4e from 3000 to 3400 s. (**f**) Performance output of the device after using different electrodes.

The number of SDBS dip-coating cycles was also identified as a key factor affecting the output performance. Figure 4b displays the variation in short-circuit current with different numbers of SDBS dip-coating cycles (with the CNT coating fixed at three cycles). The short-circuit current of the HAMEGs gradually increased with the number of SDBS coatings and stabilized after the fourth cycle. This suggests that increased SDBS loading enhances the membrane's hygroscopicity, enabling the adsorption of more moisture and the release of more cations, thereby strengthening the ion concentration gradient and improving the device performance. In the absence of SDBS coating, no significant electrical signal was observed, highlighting its crucial role in moisture-induced

electricity generation. Considering both experimental efficiency and performance, three cycles of SDBS coating were selected for subsequent experiments.

The number of CNT dip-coating cycles also significantly influenced the output signal (Figure 4c). As the number of CNT coatings increased, the device resistance gradually decreased (see Figure S10), and the current correspondingly strengthened. With no or only one CNT coating, the device exhibited almost no output, likely due to an unoptimized pore structure and high internal resistance (>60 MΩ), which slowed ion migration and hindered the effective collection of the ionic current. This result indicates that optimizing internal resistance is essential for generating detectable electrical signals in horizontally structured electrospun MEGs. A significant current increase was observed when the number of coatings reached five. Considering the balance between performance and structural integrity, three cycles of CNT coating were chosen for further study.

The output performance was also closely related to the ambient humidity (Figure 4d). The HAMEG showed almost no response at low humidity (15% RH). A measurable current began to be generated when the humidity increased to 43% RH and rose continuously with increasing humidity, reaching a maximum at 93% RH, demonstrating the device's excellent humidity response. Moreover, the output signal changed rapidly in response to humidity variation (Figure 4e), further confirming the significant influence of ambient humidity and the device's high sensitivity. The effect of temperature on the output performance of HAMEG was also preliminarily examined (see Figure S11). Additionally, different electrode materials were found to affect the output performance (Figure 4f).

Based on the experimental results, the working mechanism of the device is proposed as follows: When exposed to a humid environment, the SDBS side absorbs moisture and dissociates, releasing cations such as Na^+ and H^+, thereby establishing an ion concentration gradient across the device [28]. Simultaneously, an electric double layer forms at the negatively charged solid-liquid interface of the membrane, promoting the directional migration of cations and generating an electrical signal. A schematic of this mechanism is shown in Figure 5a: Under the combined action of CNTs and SDBS, the membrane structure becomes more compact, and the channels are negatively charged. Due to the asymmetric structure, a significant difference in hygroscopicity exists between the two sides. Upon exposure to a humid environment, the SDBS-modified side preferentially absorbs moisture and undergoes ionization, thereby establishing a macroscopic ion concentration gradient across the device. Ions migrate together with water diffusion, generating the output electrical signal. This is corroborated by the observation that the device performance decreases rapidly when the SDBS side was shielded from moisture but gradually recovers when it is re-exposed (see Figure S12), confirming the critical role of SDBS in humidity response.

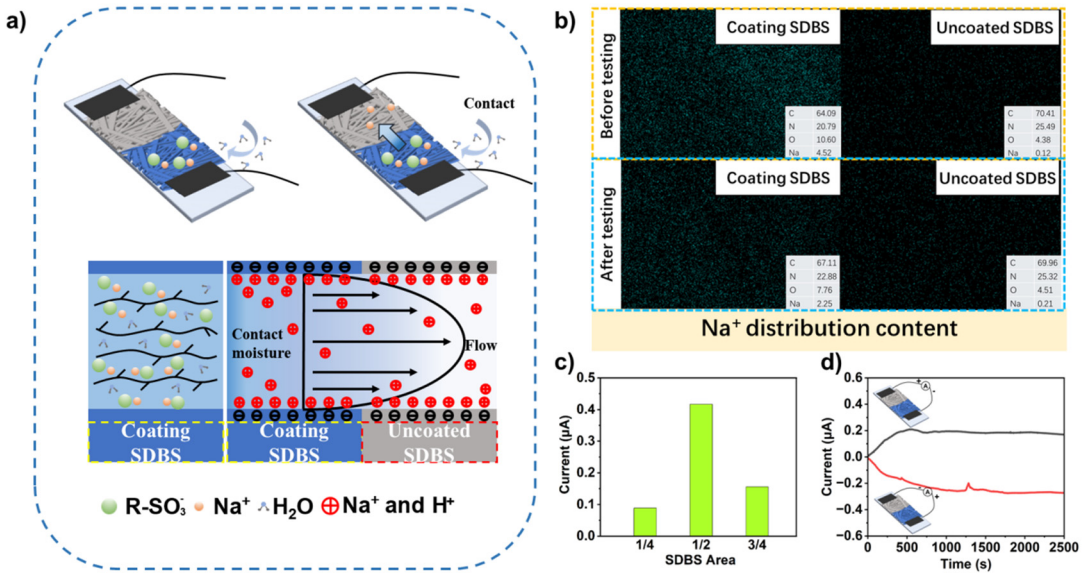

Figure 5. Mechanism and verification of HAMEG. (**a**) Speculation on the mechanism of HAMEG. (**b**) The EDS images of sodium element distribution in the device before and after testing in a humid environment. (**c**) Short-circuit output current of devices under different SDBS coverage areas. (**d**) Polarity test of HAMEG.

To verify this hypothesis, EDS characterization was performed on the device before and after exposure to humidity, as shown in Figure 5b. The corresponding SEM images are shown in Figure S13. The results indicated a significantly higher Na^+ content on the SDBS-loaded side before humidity exposure than that observed after exposure, confirming the migration of sodium ions. Concurrently, EDS analysis on the side without SDBS showed a higher sodium ion content after humidity exposure than before. Therefore, the EDS results confirm that the

electrical signal generation is attributed to the directional migration of cations such as Na^+. Specifically, SDBS determines ion generation and the driving force, while CNTs determine the effective collection and amplification of ion signals. Together, they form a complete moisture-induced power generation chain of "ion generation–directional migration–electron output". This collaborative mechanism is the key for HAMEG to achieve stable moisture-enabled electrical output. It is worth noting that SDBS and CNTs cannot function independently in the HAMEG system (Figure 4b,c). As the primary humidity-responsive ion source, SDBS establishes an asymmetric ion gradient, while CNTs construct a continuous conductive pathway and optimize the pore structure, effectively converting ion migration into stable electronic output. Therefore, the synergy between SDBS and carbon nanotubes is crucial for achieving reliable moisture-induced power generation.

To further validate the mechanism, the coverage ratio of SDBS was changed. As shown in Figure 5c, the output current was minimal when the SDBS coverage was 1/4, likely due to low SDBS loading, insufficient dissociated ion concentration, and an increased transport distance, leading to a reduced electrical signal. When the coverage was 3/4, although the SDBS content increased, the shortened ion migration distance resulted in a smaller final ion concentration difference, thereby also causing signal attenuation. When the entire membrane was covered with SDBS, the ion concentration gradient was eliminated, resulting in negligible directional ion migration and thus an electrical signal close to zero. The optimal performance was achieved with a 1/2 SDBS coverage ratio, where the ion concentration difference was maximized, and the transport distance was appropriate. This result confirms the importance of SDBS distribution for the power generation of the device.

Furthermore, a polarity test was conducted on the HAMEG to verify that the electrical signal originates from the directional migration of cations such as Na^+. As shown in Figure 5d, when the positive terminal of the measuring equipment was connected to the side of the HAMEG opposite the SDBS-modified region, a positive current signal was recorded, indicating the migration of cations from the SDBS side to the opposite side within the device. Conversely, reversing the connection, with the positive terminal connected to the SDBS side, yielded a negative current signal, further confirming that the electricity generation is caused by the directional migration of cations across the asymmetric membrane.

Based on the working mechanism of this HAMEG, its practical applications can be further extended. The device can be integrated into a commercial mask (Figure 6a) to harvest energy from the wearer's exhalation. The device demonstrated repeatable responses to exhalation signals, showing potential for energy harvesting and storage to power low-consumption wearable devices. Additionally, the device responded effectively to human touch signals (Figure 6b). Meanwhile, this device can also detect the speed of breathing; at different breathing frequencies, the short-circuit output current of the device varies (see Figure S14). Upon finger contact with the membrane surface, the output signal responded rapidly, making it highly suitable for applications such as touch switches, tactile sensors, and human-machine interaction. With future large-area fabrication and integration, this device could significantly enhance its application value and broaden its prospects.

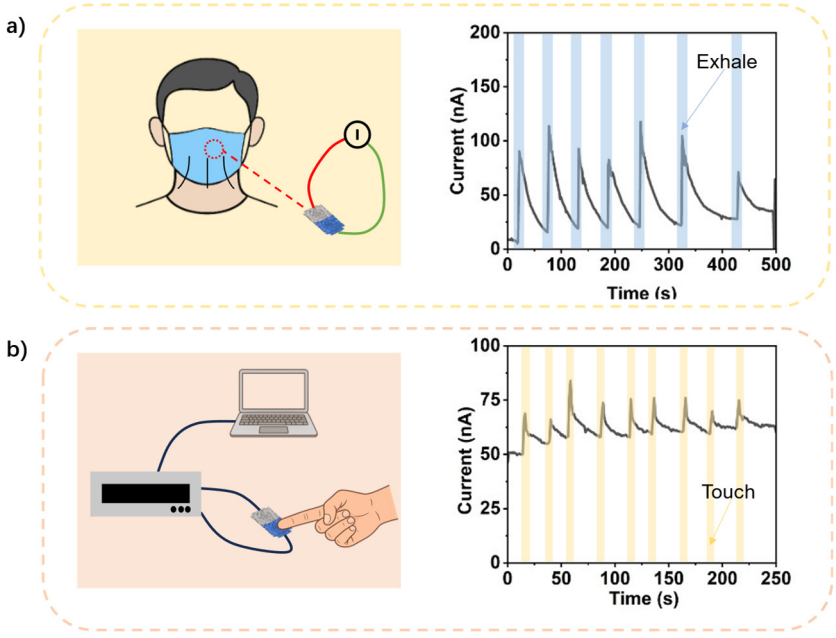

Figure 6. Application prospects of HAMEG. (**a**) Transforming the wearer's exhalation behavior into electrical signals. (**b**) Detect the contact of fingers.

4. Conclusions

In this study, we present a horizontally structured, moisture-enable electric generator based on a carbon nanotube-decorated polyacrylonitrile electrospun nanofiber membrane. In this system, PAN nanofibers provide a negatively charged porous framework for ion-selective transport, CNTs construct efficient conductive pathways, and the asymmetrically distributed SDBS serves as a moisture-responsive ion source. The synergistic interaction among these components enables stable and directional moisture-sensing electrical output. Through appropriate characterization and experiments, the working mechanism is demonstrated as follows: in a humid environment, SDBS absorbs moisture and dissociates Na^+ and H^+ ions. Driven by the resulting ion concentration gradient and electric double layer effects, these cations migrate directionally, generating an electrical output of approximately 60 mV and 3 μA at 93% RH. Compared to traditional vertical moisture-enabled generators, this horizontal configuration offers superior mechanical stability and flexible integration potential. The device functions not only as a power generator but also as an effective touch sensor, demonstrating practical versatility. Moreover, the electrospinning-impregnation approach avoids stringent ink formulation requirements of printing-based techniques (e.g., 3D/inkjet printing), enabling direct fabrication of flexible membranes with intrinsic multiscale porosity—ideal for moisture-enabled ion transport while allowing facile scaling and low-cost production. This work provides valuable insights into the design of horizontally structured, nanofiber-based moisture-electric devices.

Supplementary Materials

The additional data and information can be downloaded at: https://media.sciltp.com/articles/others/26011209 52067315/LDM-25100125-SM-FC-done.pdf. Figure S1: PAN nanofiber film. The film is flexible and can be bent and folded at will. Figure S2: SEM image of CNT distribution on the surface of PAN nanofiber films. Figure S3: XPS diagram of PAN nanofiber film impregnated with CNT. Figure S4: FTIR results of the original PAN nanofiber film and the PAN nanofiber film with SDBS. Figure S5: Power density with variable external resistance. Figure S6: On-site testing equipment. Figure S7: Humidity test environment. Figure S8: Short-circuit current output of HAMEG under different film lengths. Figure S9: Short-circuit current output of HAMEG under different film width. Figure S10: Thin-film resistors under different CNT impregnation times. Figure S11: Short-circuit current output of HAMEG under different temperature. Figure S12: The short-circuit current signal changes before and after being covered at the impregnated SDBS of the device. Figure S13: SEM image at the EDS scanning point. Figure S14: Short-circuit current output of HAMEG at different respiratory rates. Table S1: The contrast between horizontal structure and vertical structure. Table S2: A comparison of representative MEGs reported in the literature in recent years. References [11,12,17,27–29,37–42] are cited in Supplementary Materials.

Author Contributions

M.R. designed experiments and completed original draft. X.L. and C.F. provided the idea for the article. X.L. guided this research. T.Y. improved the article writing and provided the funding. All authors have read and agreed to the published version of the manuscript.

Funding

The authors acknowledge the financial supports from the National Natural Science Foundation of China (Grant Nos. 52575233).

Institutional Review Board Statement

Not applicable.

Informed Consent Statement

Not applicable.

Data Availability Statement

The data presented in this study are available from the corresponding author upon reasonable request.

Conflicts of Interest

The authors declare no conflict of interest.

Use of AI and AI-Assisted Technologies

No AI tools were utilized for this paper.

References

1. Peng, X.; Liu, Z.; Jiang, D. A Review of Multiphase Energy Conversion in Wind Power Generation. *Renew. Sustain. Energy Rev.* **2021**, *147*, 111172.
2. Hao, D.; Qi, L.; Tairab, A.M.; et al. Solar energy harvesting technologies for PV self-powered applications: A Comprehensive Review. *Renew. Energy* **2022**, *188*, 678–697.
3. Khan, N.D.; Kalair, A.; Abas, N.; et al. Review of Ocean Tidal, Wave and Thermal Energy Technologies. *Renew. Sustain. Energy Rev.* **2017**, *72*, 590–604.
4. Tan, E.; Liu, Y.; Hu, C.; et al. Low-Humidity-Dependent and Stretchable Moisture-Electricity Generator Based on $Ti_3C_2T_x$ MXene-Loaded Cotton and Hydrogel Bilayer for Green Power Harvesting and Wearable Electronics. *ACS Appl. Mater. Interfaces* **2025**, *17*, 48375–48386.
5. Liang, Y.; Zhao, F.; Cheng, Z.; et al. Electric Power Generation via Asymmetric Moisturizing of Graphene Oxide for Flexible, Printable and Portable Electronics. *Energy Environ. Sci*. **2018**, *11*, 1730–1735.
6. Qu, Y.; Zhang, X.; Fu, Q.; et al. Fabrication of High-Performance Moisture-Electric Generators via Synergistic Effect between CNTs and TiO_2 on Porous PU Structure. *Compos. Sci. Technol*. **2023**, *241*, 110105.
7. Zhao, F.; Cheng, H.; Zhang, Z.; et al. Direct Power Generation from a Graphene Oxide Film under Moisture. *Adv. Mater.* **2015**, *27*, 4351–4357.
8. Huang, Y.; Cheng, H.; Shi, G.; et al. Highly Efficient Moisture-Triggered Nanogenerator Based on Graphene Quantum Dots. *ACS Appl. Mater. Interfaces* **2017**, *9*, 38170–38175.
9. Shen, D.; Xiao, M.; Zou, G.; et al. Self-Powered Wearable Electronics Based on Moisture Enabled Electricity Generation. *Adv. Mater*. **2018**, *10*, 1705925.
10. Huang, Y.; Cheng, H.; Yang, C.; et al. All-Region-Applicable, Continuous Power Supply of Graphene Oxide Composite. *Energy Environ. Sci*. **2019**, *12*, 1848–1856.
11. Lyu, Q.; Peng, B.; Xie, Z.; et al. Moist-Induced Electricity Generation by Electrospun Cellulose Acetate Membranes with Optimized Porous Structures. *ACS Appl. Mater. Interfaces* **2020**, *12*, 57373–57381.
12. Zhang, J.; Zhuang, J.; Lei, L.; et al. Rapid Preparation of a Self-Adhesive PAA Ionic Hydrogel Using Lignin Sulfonate–Al^{3+} Composite Systems for Flexible Moisture-Electric Generators. *J. Mater. Chem. A* **2023**, *11*, 3546–3555.
13. Yang, S.; Tao, X.; Chen, W.; et al. Ionic Hydrogel for Efficient and Scalable Moisture-Electric Generation. *Adv. Mater*. **2022**, *34*, 2200693.
14. Cai, T.; Lan, L.; Peng, B.; et al. Bilayer Wood Membrane with Aligned Ion Nanochannels for Spontaneous Moist-Electric Generation. *Nano Lett*. **2022**, *22*, 6476–6483.
15. Ren, G.; Wang, Z.; Zhang, B.; et al. A Facile and Sustainable Hygroelectric Generator Using Whole-Cell Geobacter Sulfurreducens. *Nano Energy*. **2021**, *89*, 106361.
16. Xu, T.; Ding, X.; Huang, Y.; et al. An Efficient Polymer Moist-Electric Generator. *Energy Environ. Sci*. **2019**, *12*, 972–978.
17. Wang, H.; Sun, Y.; He, T.; et al. Bilayer of Polyelectrolyte Films for Spontaneous Power Generation in Air up to an Integrated 1,000 V Output. *Nat. Nanotechnol*. **2021**, *16*, 811–819.
18. Huang, G.; Liu, J.; Zhang, H.; et al. A Double-Gradient Structured Hydrogel for an Efficient Moisture-Electric Generator. *Chem. Eng. J*. **2025**, *504*, 158878.
19. Yang, S.; Zhang, L.; Mao, L.; et al. Green Moisture-Electric Generator Based on Supramolecular Hydrogel with Tens of Milliamp Electricity toward Practical Applications. *Nat. Commun*. **2024**, *15*, 3329.
20. Sun, Z.; Feng, L.; Wen, X.; et al. Nanofiber Fabric Based Ion-Gradient-Enhanced Moist-Electric Generator with a Sustained Voltage Output of 1.1 Volts. *Mater. Horiz.* **2021**, *8*, 2303–2309.
21. Wang, Z.; Li, J.; Shao, C.; et al. Moisture Power in Natural Polymeric Silk Fibroin Flexible Membrane Triggers Efficient Antibacterial Activity of Silver Nanoparticles. *Nano Energy* **2021**, *90*, 106529.
22. Li, T.; Li, L.; Sun, H.; et al. Porous Ionic Membrane Based Flexible Humidity Sensor and Its Multifunctional Applications. *Adv. Sci*. **2017**, *4*, 1600404.
23. Yang, B.; Aksak, B.; Lin, Q.; et al. Compliant and Low-Cost Humidity Nanosensors Using Nanoporous Polymer Membranes. *Sens. Actuators B: Chem.* **2006**, *114*, 254–262.
24. Zhang, Y.; Zhang, T.; Huang, Z.; et al. A new class of electronic devices based on flexible porous substrates. *Adv. Sci*. **2022**, *9*, 2105084.
25. Hu, Y.; Yang, W.; Wei, W.; et al. Phyto-Inspired Sustainable and High-Performance Fabric Generators via Moisture Absorption-Evaporation Cycles. *Sci. Adv*. **2024**, *10*, eadk4620.
26. Chen, T.; Jiang, X.; Qiang, S.; et al. Construction of Cellulose-Based Dual-Gradient Heterogeneous Bilayer Membranes

with Optimized Directional Moisture Transport Property for Enhancing Moisture-Electricity Generation. *Int. J. Biol. Macromol*. **2025**, *307*, 142060.
27. Zheng, H.; Zhou, A.; Li, Y.; et al. A Sandwich-like Flexible Nanofiber Device Boosts Moisture Induced Electricity Generation for Power Supply and Multiple Sensing Applications. *Nano Energy* **2023**, *113*, 108529.
28. Sun, Z.; Wen, X.; Wang, L.; et al. Capacitor-Inspired High-Performance and Durable Moist-Electric Generator. *Energy Environ. Sci*. **2022**, *15*, 4584–4591.
29. Fauziah, A.R.; Schöfbeck, F.; Reithofer, M.R.; et al. Self-Powered Flexible Janus-like Metal-Organic Framework Membrane for Sustainable Moisture-Enabled Electrokinetic Energy Harvesting. *J. Mater. Chem. A*. **2026**. https://doi.org/10.1039/D5TA06289F.
30. Patel, D.K.; Patil, T.V.; Ganguly, K.; et al. Nanocellulose-Assisted 3D-Printable, Transparent, Bio-Adhesive, Conductive, and Biocompatible Hydrogels as Sensors and Moist Electric Generators. *Carbohydr. Polym*. **2023**, *315*, 120963.
31. Huang, Y.; Zhou, K.; Cheng, H.; et al. Three-Dimensional Printing of High-Performance Moisture Power Generators. *Adv. Funct. Mater*. **2024**, *34*, 2308620.
32. He, T.; Wang, H.; Lu, B.; et al. Fully Printed Planar Moisture-Enabled Electric Generator Arrays for Scalable Function Integration. *Joule* **2023**, *7*, 935–951.
33. Anagnostou, K.; Urban, M.; Sotiropoulos, E.; et al. Water-Based Graphene Oxide Inks for Inkjet-Printed Flexible Moisture Energy Generators. *Sci. Rep*. **2025**, *15*, 24685.
34. Yang, Y.; Xu, Y.; Liu, Z.; et al. Preparation and Characterization of High-Performance Electrospun forward Osmosis Membrane by Introducing a Carbon Nanotube Interlayer. *J. Membr. Sci*. **2020**, *616*, 118563.
35. Pérez-Álvarez, L.; Ruiz-Rubio, L.; Moreno, I.; et al. Characterization and Optimization of the Alkaline Hydrolysis of Polyacrylonitrile Membranes. *Polymers* **2019**, *11*, 1843.
36. Zhang, X.; Liu, X.; Jiang, L. Wettability and Applications of Nanochannels. *Adv. Mater*. **2019**, *31*, 1804508.
37. Zhang, Y.; Guo, S.; Yu, Z.G.; et al. An Asymmetric Hygroscopic Structure for Moisture-Driven Hygro-Ionic Electricity Generation and Storage. *Adv. Mater*. **2022**, *34*, 2201228.
38. He, H.; Zhang, J.; Pan, J.; et al. Moisture-Enabled Electric Generators Based on Electrospinning Silk Fibroin/Poly (Ethylene Oxide) Film Impregnated with Gradient-Structured Sericin. *ACS Appl. Energy Mater*. **2024**, *7*, 2980–2988.
39. Zhao, K.; Li, S.; Zan, G.; et al. Moisture-Driven Energy Generation by Vertically Structured Polymer Aerogel on Water-Collecting Gel. *Nano Energy* **2024**, *126*, 109645.
40. Sun, Z.; Feng, L.; Xiong, C.; et al. Electrospun Nanofiber Fabric: An Efficient, Breathable and Wearable Moist-Electric Generator. *J. Mater. Chem. A* **2021**, *9*, 7085–7093.
41. Wang, L.; Feng, L.; Sun, Z.; et al. Flexible, Self-cleaning, and High-Performance Ceramic Nanofiber-Based Moist-Electric Generator Enabled by Interfacial Engineering. *Sci. China Technol. Sci*. **2022**, *65*, 450–457.
42. Akhtar, M.S.; Li, Z.Y.; Park, D.M.; et al. A New Carbon Nanotubes (CNTs)–Poly Acrylonitrile (PAN) Composite Electrolyte for Solid State Dye Sensitized Solar Cells. *Electrochim. Acta* **2011**, *56*, 9973–9979.